Shell- and subshell-resolved projectile excitation of hydrogenlike Au^{78+} ions in relativistic ion-atom collisions

A. Gumberidze,[1,2,*] S. Fritzsche,[2,3,4] F. Bosch,[3] D. C. Ionescu,[5] A. Krämer,[3] C. Kozhuharov,[3] Z. Stachura,[6] A. Surzhykov,[3,7] A. Warczak,[8] and Th. Stöhlker[1,3,7]

[1]*ExtreMe Matter Institute EMMI and Research Division, GSI Helmholtzzentrum für Schwerionenforschung, D-64291 Darmstadt, Germany*
[2]*Frankfurt Institute for Advanced Studies FIAS, D-60438 Frankfurt am Main, Germany*
[3]*GSI Helmholtzzentrum für Schwerionenforschung, D-64291 Darmstadt, Germany*
[4]*Department of Physics, Post Office Box 3000, FIN-90014 University of Oulu, Finland*
[5]*Portland House, 8 Collins Street 3000 Melbourne, Australia*
[6]*Institute for Nuclear Physics, 31-342 Kraków, Poland*
[7]*Physikalisches Institut, Ruprecht-Karls-Universität Heidelberg, Germany*
[8]*Institute of Physics, Jagiellonian University, Krakow, Poland*

(Received 29 July 2010; published 30 November 2010)

The projectile excitation of high-Z ions has been investigated in relativistic ion-atoms collisions by observing the subsequent x-ray emission. The x-ray spectra from the projectile excitation have been separated from the x-ray emission following electron capture into the excited states using a novel anticoincidence technique. For the particular case of hydrogenlike Au^{78+} ions colliding with Ar atoms, Coulomb excitation from the ground state into the fine-structure-resolved $n = 2$ levels as well as into levels with principal quantum number $n \geqslant 3$ has been measured with excellent statistics. The observed spectra agree well with simulated spectra that are based on Dirac's relativistic equation and the proper inclusion of the magnetic interaction into the amplitudes for projectile excitation. It is shown that a coherent inclusion of the magnetic part of the Lienard-Wiechert potential leads to the lowering of the excitation cross section by up to 35%. This effect is more pronounced for excitation into states with high angular momentum and is confirmed by our experimental data.

DOI: 10.1103/PhysRevA.82.052712 PACS number(s): 34.50.Fa, 32.30.Rj

I. INTRODUCTION

Relativistic ion-atom collisions, when followed by characteristic (radiative) transitions have been found to be of great importance for studying the elementary processes of light-matter interaction in the presence of strong Coulomb fields. In addition to high-resolution QED studies for highly charged ions [1,2], ion-electron and ion-atom collisions with high-Z ions have helped to explore the dynamical aspects of the electron-photon interaction in great detail [3–5]. Especially for the highest projectile charge states, the experimental storage ring (ESR) in Darmstadt, but also the electron beam ion traps (EBIT) provide unique conditions for exploring nonradiative, radiative, or dielectronic capture and recombination processes [6–12] thus allowing for valuable tests of theoretical models. For the case of electron capture studies at the ESR, most of the experimental investigations were based on x-ray spectroscopic techniques where the x-ray emission from the projectile ions is detected in coincidence with the down-charged projectile after the collision. Because of the large fine-structure splitting at high-Z, these studies revealed subtle details for the capture mechanism, such as the alignment of the excited states formed in the course of the collisions [13–16] or the linear polarization of recombination transitions [14,17,18]. Recently, moreover, similar studies have been reported for the case of K-shell ionization of few-electron projectiles where, for the case of initial Li-like ions, a selective population of excited s states has been found [19,20].

In contrast to electron capture, however, the experimental information about the Coulomb excitation of high-Z few-electron ions in relativistic ion-atom collisions where the perturbation by the Coulomb potential of the target nucleus leads to the excitation of the projectile electron has remained, so far, rather scarce. This is in contrast to the low-Z [21–23] and mid-Z ranges [24–29] where quite detailed information has been obtained experimentally. In addition, a series of measurements have been carried out at the EBIT facilities where electron impact excitation has been investigated for different elements [30,31].

The formation of excited states via Coulomb excitation in collisions with atomic targets can be studied for highly charged ions by observing, for instance, their characteristic decay back into the ground state. For hydrogenlike bismuth, especially, these x-ray spectra have been observed by Stöhlker and coworkers [32,33]. In these studies, the total cross sections for the K-shell excitation of hydrogenlike and heliumlike ions were explored. The evidence was found in these experiments that the magnetic part of the Lienard-Wiechert interaction leads to a reduction of the total cross sections by about 30% which has triggered more detailed theoretical studies [34–37]. The similarity of Coulomb excitation with Coulomb ionization of high-Z projectiles in relativitic collisions with low-Z targets [38] is of especially great interest since Coulomb ionization is one of the most important charge-exchange channels in ion-atom collisions for which a large body of experimental data is available [39–45].

The systematic deviation of all experimental data on the Coulomb ionization from first-order perturbation theory [41] is remarkable, an issue which has not been resolved so far. In contrast to ionization, the final state of an excitation of one (or

*a.gumberidze@gsi.de

more) electrons can be controlled much better experimentally and thus more detailed information can be deduced from the measurements. However, experimental difficulties in studying excitation processes arise from the fact that an excitation does not change the charge state of the projectile. In conventional collision experiments, it is therefore rather difficult to separate the characteristic projectile x-ray emission from other x-ray production processes, such as the secondary electron bremsstrahlung which can be quite an intense source of background, in particular when solid targets are used.

In the present work, we extended the former studies on the K-shell projectile excitation by exploiting the unique, almost background-free conditions at the internal gas target of the ESR storage ring. This pilot experiment was conducted for hydrogenlike gold ions in collision with an argon gas target at an energy of 258 MeV/u. Most importantly, the background-free conditions enabled us to introduce a new, the so-called *anticoincidence*, technique. This anticoincidence technique was used to separate the characteristic projectile photons due to the Coulomb excitation from the x-ray spectra due to electron capture. The application of this technique at the ESR storage ring allowed us to obtain clean and intense x-ray spectra due to the excitation process and thus significantly improved the experimental precision compared to the former studies. In particular, the excitation of the K-shell electron into the shells with $n \geqslant 3$ have been observed and are compared with simulated spectra. A relativistic formalism, based on Dirac's equation, was applied to evaluate the excitation amplitudes. Excellent agreement between the observed and simulated spectra are obtained if the cascade dynamics for all states with $\leqslant$10 and the complete Liénard-Wiechert interaction are taken into account. The calculations show a substantial but subshell-dependent reduction of the cross sections when compared to a quasirelativistic approach, in which the magnetic contributions are neglected or added incoherently.

The paper is organized as follows. In the next section, we first report about the measurements which has been carried out with a beam of hydrogenlike gold ions at the ESR storage ring. To further analyze the observed spectra, calculations have been performed for both the $1s \rightarrow nl_j$ excitation cross sections and their subsequent decay cascades. In Sec. III, we outline the basic theory and describe the calculations in more detail. Simulated spectra from different computational models are compared with experiment and discussed in Sec. IV. Finally, a few conclusions are drawn in Sec. V.

II. EXPERIMENT

The experiment was performed at the ESR by using H-like Au ions delivered by the heavy ion synchrotron (SIS) at an energy of 258 MeV/u. An efficient electron cooling in the ESR storage ring provided beams with very low emitance (beam size of less then 5 mm) and a longitudinal momentum spread of $\Delta p/p \sim 10^{-5}$ which enabled storage of the beam with long lifetimes as well as a decrease of the uncertainties due to the relativistic Doppler effect. After the accumulation of the ions in the ring and their subsequent cooling, the ion beams interacted with a supersonic jet of Ar target atoms. For the experiment, the atomic physics photon detection chamber at the internal target of the ESR was utilized [46]. The x rays from the excited projectile states, produced in collisions of the stored ion beams with the jet target, were detected by two planar solid state Ge(i) detectors, mounted at the observation angles of 35° and 150° with respect to the beam axis. The detectors were separated from the ultrahigh vacuum (UHV) of the ring by 100-μm thick Be windows. Those projectile ions that captured one electron were observed after the next dipole magnet with a multiwire proportional counter (MWPC). The x rays were recorded in a (so-called) single mode in which no hardware coincidence condition need to be fulfilled. Instead, every x-ray photon is first accepted as a trigger to read out the energy and time information of all detectors provided by the analog to digital converter (ADC) and time to digital converter (TDC) modules. In this way, the coincidence information between the emitted x rays and the ions which have captured one electron has also been acquired.

In Fig. 1(a), we display the single-mode total spectra, measured without any coincidence condition at 35°, in which the

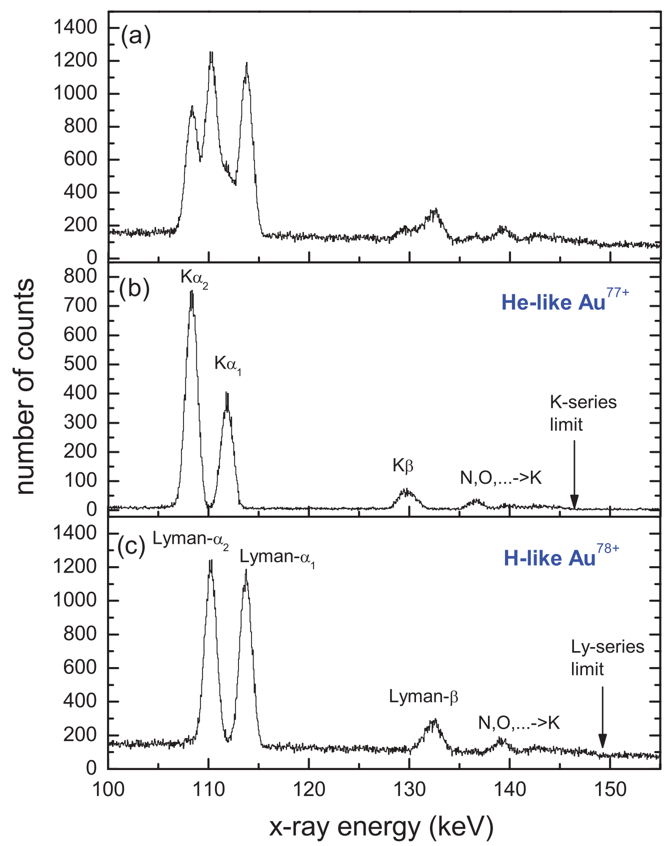

FIG. 1. (Color online) (a) X-ray spectrum, measured without any coincidence condition, in collisions of H-like Au ions with Ar target at 258 MeV/u, at 35° observation angle with respect to the ion beam. Here the characteristic radiation at around 110 keV arises from both the electron capture (i.e., the subsequent Kα transitions in He-like gold) and the excitation of the H-like gold ions (Ly-α transitions). (b) X-ray spectrum due to the capture of an electron into the initially H-like Au projectile, in coincidence with measuring He-like Au ions. Indeed, only the Kα transitions of He-like gold can be seen. (c) X-ray spectrum obtained in anticoincidence with the electron capture. Here characteristic transitions into the K shell of H-like gold due to excitation are present. Note that due to the relativistic Doppler effect the characteristic lines of gold are shifted and appear at around 110 keV in the laboratory frame under a 35° angle.

characteristic x-ray photons arise from both the Kα emission of He-like gold following the electron capture and the Ly-α transitions after an excitation of the H-like gold projectiles. Figure 1(b) shows the x-ray spectrum that is associated with the capture of one electron by the initially H-like Au projectiles, forming He-like Au ions. This spectrum can be obtained by exploiting the coincidence time information recorded during the measurement. In the coincidence spectrum, indeed, only the Kα transitions in He-like gold can be seen. Furthermore, by subtracting the latter spectrum (with the coincidence condition included) from the total (single-mode) one, we obtain the spectrum in anticoincidence with the electron capture, as displayed in Fig. 1(c). Apart from the background, that mainly arises from bremsstrahlung, this spectrum contains the characteristic lines associated only with the excitation of the H-like gold ions in collisions with Ar atoms. Note that although the energy resolution of the experimental setup is not sufficient to fully resolve the transitions of the H-like and He-like gold projectile ions, we were able to obtain a clean x-ray spectra associated only with the Coulomb excitation of the projectiles by utilizing the anticoincidence technique. This spectrum can be used for further evaluation to obtain quantitative information about the excitation process in relativistic collisions.

III. THEORY AND COMPUTATIONS

To understand and interpret the observed x-ray spectra we need to model the excitation (cross sections) for populating the excited projectile states as well as their subsequent decay (cascades). While the radiative decay of few-electron ions and depopulation of their excited states are quite well understood in terms of rate equations (see Sec. III C), further effort is required to calculate (Coulomb) excitation cross sections for fast ions. Note in the following we omit completely the process of electron impact excitation. Coulomb excitation caused by the nuclear charge Z_T of the target scales with Z_T^2 whereas the cross section for electron impact excitation scales linearly with the amount of target electrons available. For the particular case of Ar as target atom we expect that electron impact excitation contributes only by a few percent to the overall excitation cross section.

In the following sections, we first summarize the semiclassical theory for the excitation of relativistic projectiles (Sec. III A) and describe how the required amplitudes can be evaluated by using an algebraic representation of the wave functions (Sec. III B). In Sec. III C, finally, we outline how these amplitudes are utilized for the simulation of (theoretical) x-ray spectra that can be compared directly with observations.

A. Excitation cross sections for fast ions

For fast projectiles, a semiclassical impact parameter picture is appropriate in which the (heavy) ions move along a "classical" straight-line trajectory, independent of the motion of the electron at both the target as well as the projectile. For reference, we choose coordinates where the projectile (nucleus) remains at rest at the origin and where the target moves with constant velocity $\mathbf{v} = v\mathbf{e}_z$ along the z axis. In these coordinates, an excitation of the projectile electron occurs first of all due to the fast-moving potential of the target nucleus. As "seen" by the projectile, this is a Liénard-Wiechert potential (for the x-z scattering plane)

$$(A^0,\mathbf{A}) = \gamma \frac{\alpha Z_T}{r'}(1, 0, 0, +\beta), \tag{1}$$

and includes both the electric (first) and magnetic (last) components. In this definition of the Liénard-Wiechert potential, $\alpha \simeq 1/137$ is the fine-structure constant, $\beta = v/c$, $\gamma = (1-\beta^2)^{-1/2}$, and Z_T is the charge of the target nucleus. The time-dependent parameter $r' = \sqrt{(x-b)^2 + y^2 + \gamma^2 (z-vt)^2}$ denotes the distance of the target from the projectile electron as seen in the given reference frame. Here and in the following formulas we use natural units ($\hbar = m_e = c = 1$). In first-order perturbation theory, the transition amplitude for exciting the projectile electron at a fixed impact parameter b is then given by [9,47]

$$A_{fi}(b) = i\,\gamma\,\alpha\,Z_T \int dt\, e^{i(E_f - E_i)t} \times \int d^3\mathbf{r}\, \psi_f^\dagger(\mathbf{r}) \frac{1-\beta\,\hat{\alpha}_z}{r'}\, \psi_i(\mathbf{r}), \tag{2}$$

with $[\psi_i(\mathbf{r}), E_i]$ and $[\psi_f(\mathbf{r}), E_f]$ being the wave functions and total energies of the initial and final states of the projectile electron, respectively. In the transition amplitude (2), the space-like component A^3 of the Liénard-Wiechert potential [cf. Eq. (1)] gives rise to a *magnetic part* which is proportional to the Dirac matrix $\hat{\alpha}_z$.

The cross section for an excitation of the projectile electron from state $|i\rangle \to |f\rangle$ is determined by the b-dependent probability $P(b) = |A_{fi}(b)|^2$ and obtained by integration over all impact parameters b. If we introduce, in addition, the minimum momentum transfer $q_o = (E_f - E_i)/v$, the integration over the time t in Eq. (2) can be carried out analytically

$$\begin{aligned}\sigma_{fi} &= 2\pi \int_0^\infty db\, b\, P_{fi}(b)\\ &= 8\pi \frac{\alpha^2 Z_T^2}{v^2} \int db\, b \Big| \langle \psi_f | (1-\beta\,\hat{\alpha}_z)\, e^{iq_0 z} \\ &\quad \times K_0\Big(\frac{q_0}{\gamma}\sqrt{(x-b)^2 + y^2}\Big) |\psi_i\rangle \Big|^2,\end{aligned} \tag{3}$$

where $K_0(x)$ denotes the modified Bessel function. Details about this time integration can be found in Ref. [9], but as seen already from expression (3), the effective interaction of the projectile electron extends up to about $1/q_0$ parallel to the z axis along the beam and up to γ/q_0 perpendicular to it (i.e., within the scattering plane). This dependence is very characteristic for the behavior of Liénard-Wiechert interactions.

For high-Z, hydrogenlike projectiles in the $|i\rangle = |1s,m_i\rangle$ ground state, the cross section (3) can be evaluated for any excited state $|f\rangle = |n_f \kappa_f m_f\rangle$ once a proper set of Dirac orbitals is available. However, since the modified Bessel function $K_0(x)$ cannot so easily be written in terms of spherical tensors, it is more convenient in this case to perform the three-dimensional integration over the spatial coordinates

(r,ϑ,φ) explicitly, in addition to the integration over the impact parameter b.

B. Algebraic representation of wave functions

To keep the four-dimensional integration in the expression (3) for the cross section (3) feasible, a basis set approach has been applied here to represent the (one-electron) Dirac orbitals for a given central field of the nucleus

$$\psi_{n\kappa m}(\mathbf{r}) = \frac{1}{r}\begin{bmatrix} P_{n\kappa}(r)\,\Omega_{\kappa\,m}(\theta,\phi) \\ i\ \ Q_{n\kappa}(r)\,\Omega_{-\kappa\,m}(\theta,\phi) \end{bmatrix}. \tag{4}$$

As usual, these orbitals are classified by means of the principal quantum number n, the (relativistic) angular momentum quantum number $\kappa = \pm(j+1/2)$ for $l = j \pm 1/2$, as well as the magnetic quantum number m. While the (two-component) spherical spinors $\Omega_{\kappa\,m}(\theta,\phi)$ are known analytically [48], the two radial functions $P_{n\kappa}(r)$ and $Q_{n\kappa}(r)$, often called the large and small components, respectively, are typically evaluated numerically, either on a radial grid (finite-difference method) or by applying some proper basis set.

In the present work, approximate solutions to the radial Dirac equation

$$\begin{aligned} P_{n\kappa}(r) &= \sum_{j=1}^{N} X_{n\kappa}^{Lj}\ \ g_{\kappa j}^{L}(r), \\ Q_{n\kappa}(r) &= \sum_{j=1}^{N} X_{n\kappa}^{Sj}\ \ g_{\kappa j}^{S}(r), \end{aligned} \tag{5}$$

have been determined by using a (global) Gaussian basis with

$$g_{\kappa j}^{L}(r) = N_{\kappa j}^{L}\, r^{l+1}\, e^{-\alpha_j r^2}, \quad j = 1,\ldots,N, \tag{6}$$

$$g_{j}^{S}(r) = \left[-\frac{d}{dr} + \frac{\kappa}{r}\right] g_{j}^{L}(r), \tag{7}$$

with $N_{\kappa j}^{L}$ being a normalization constant and l the orbital angular momentum (quantum number). Moreover, the (strict) kinetic-balance condition [49] has been applied for the basis functions of the small component to ensure the proper nonrelativistic limit of the one-electron functions if $c \to \infty$. Such a basis-set representation of the radial components has the advantage that, once the coefficients $\{X_{\kappa}^{Lj}, X_{\kappa}^{Sj}, j = 1,\ldots,N\}$ are determined for a given (nuclear) potential and symmetry κ of the one-electron orbitals, the full wave function can be obtained quite easily at any point $\mathbf{r}$ in space without further interpolation and as appropriate for a (finite-order) Gaussian integration [50].

A Gaussian basis (6) and (7) is also suitable to model an extended nucleus and the subshells (states) with $n \leqslant 8,\ldots,10$ by using a moderate number of basis functions, say $N \lesssim 50$. Typically, however, subshell states with a higher principal quantum number $n \gtrsim 6$ are slightly less well represented since, for high n, the diagonalization of the Hamiltonian matrix results in *pseudo states* which describe rather the *averaged* behavior of the respective "part" of the Dirac spectrum (wave packet). This *pseudo character* of the high-n solutions is in line with the experimental setup for which excitations into subshells with $n > 6$ cannot be resolved and give rise only to corrections to the observed x-ray spectra.

Several tests were performed to understand the quality of the Dirac orbitals within the chosen basis. Good agreement with previous excitation cross sections, based on finite-difference computations, were obtained especially for hydrogenlike bismuth projectiles at 82 and 119 MeV/u laboratory energies [32].

C. Rate equations to simulate the x-ray emission

Apart from the excitation cross sections for the low-lying subshells with $n \lesssim 10$, we have calculated the decay rates of these levels (to any of the lower-lying levels) to simulate the x-ray emission of the excited ions in terms of rate equations. In such a model, the excitation cross sections provide the relative initial population of the excited levels, and their cascade follows all the possible decay pathes down toward the ground state. More specifically, the excited levels stabilize themselves by a cascade of radiative transitions whose decay dynamics are well described by a system of rate equations

$$\frac{dN_i}{dt} = -\sum_{j}^{(<)} \lambda_{ij}\, N_i + \sum_{k}^{(>)} \lambda_{ki}\, N_k \quad \forall\, i = 1,\ldots,\Lambda. \tag{8}$$

In these equations λ_{ij} denotes the decay rate from level i to level j and Λ is the total number of excited levels which are considered in the decay cascade; the index j runs over all levels with total energy $E_j < E_i$ and k over all those with $E_k > E_i$. Apart from its (exponential) decay into lower-lying levels, each level will also be "feeded" from levels having higher energies. Note for λ_{ij} exact relativistic transition rates have been used. For more information of the cascade simulation we refer to Refs. [8,51,52].

IV. RESULTS AND DISCUSSION

X-ray spectra have been recorded following the Coulomb excitation of hydrogenlike Au^{78+} ions in collision with an Ar jet target. To understand the observed spectra and analyze the underlying excitation process of the projectiles, simulations were performed for the excitation of the ions and their x-ray emission. While the (partial) cross sections for an excitation of the $1s$ electron give rise to the (initial) population of the nlj states for the projectiles after the collision, a comparison with the experiment can be made only if, in addition, their subsequent decay (cascade) is taken into account as well.

For the $1s$ ground state of hydrogenlike Au^{78+} ions, only excitations from one subshell state with, say, $|1s, m_s = +1/2\rangle$ need to be considered owing to the symmetry of the system. In first-order perturbation theory, moreover, we have $\sigma_{if} \propto Z_T^2$, and it is thus sufficient to perform calculations for proton impact. This approximation is appropriate especially for light and medium target atoms for which both the screening of the nuclear charge as well as the velocity of the inner-shell electrons is negligible compared with the ion velocity v [53].

Figure 2(a) displays the theoretical cross sections for the $1s$ excitation of hydrogenlike Au^{78+} projectiles into the low-lying subshells with $n = 2,\ldots,10$ and orbital angular momenta $l \leqslant 2$ in 258 MeV/u collisions with protons [35]. Partial cross sections, as a function of the principal

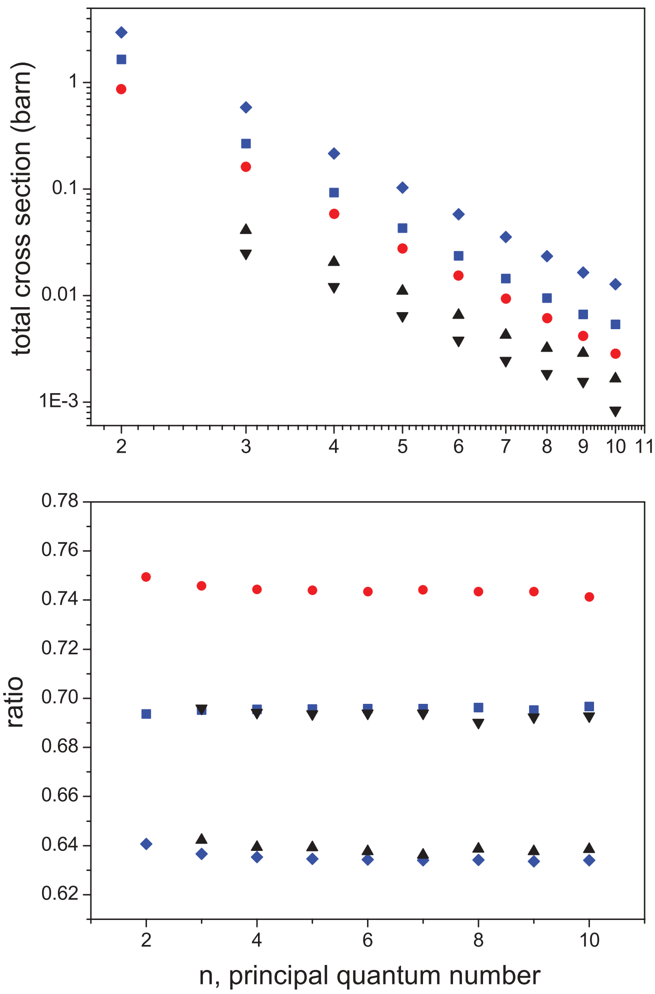

FIG. 2. (Color online) Theoretical cross sections for the $1s$ excitation of hydrogenlike Au^{78+} projectiles into the low-lying subshells with $n = 2, \ldots, 10$ and $l \leqslant 2$ in 258 MeV/u collisions with protons. Top: Partial cross section into the subshells $s_{1/2}$ (red circles), $p_{1/2}$ (blue squares), $p_{3/2}$ (blue diamonds), $d_{3/2}$ (black down-triangles), and $d_{5/2}$ (black up-triangles). Bottom: Ratio of the partial cross sections σ_{fi}(full interaction)/σ_{fi}(electric part only); see text for further discussion.

quantum number n are shown for the excitation into the five subshells $s_{1/2}$, $p_{1/2}$, $p_{3/2}$, $d_{3/2}$, and $d_{5/2}$, respectively. These cross sections were obtained as an integral over the weighted excitation probability $P(b)\, b/Z_T^2$ that peaks, depending on the particular subshell of the excited state, between 500 and about 3000 fm (i.e., well inside of the K-shell radius of the target). A typical probability distribution was shown in Ref. [32] for the projectile excitation of hydrogenlike Bi^{82+} ions.

To understand the importance of the magnetic interactions for the excitation of high-Z projectiles [i.e., the importance of the magnetic term $\sim -\beta\,\alpha_z$ in Eq. (2)] Fig. 2(b) shows the ratio of the partial excitation cross sections σ_{fi}(full interaction)/σ_{fi}(electric part only) for the full Liénard-Wiechert potential and if only the electric part is taken into account. A clear reduction of the partial cross sections due to this magnetic coupling of the fast ion and the target nucleus is found for all subshells. At the (relativistic) energy of 258 MeV/u of the projectile ions, especially, the

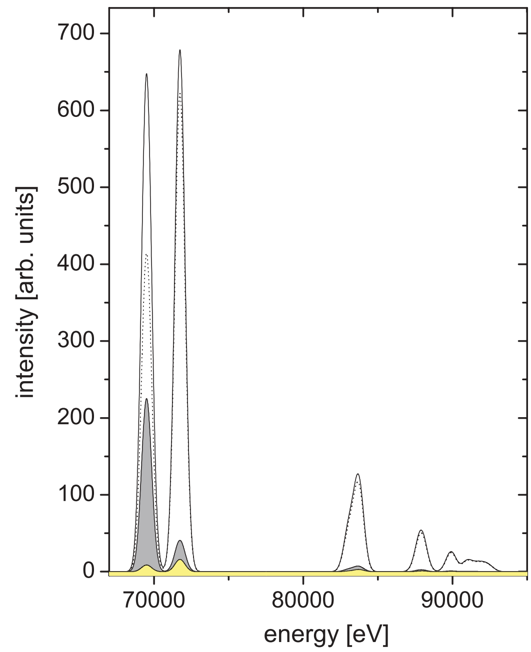

FIG. 3. (Color online) Simulated Lyman series in hydrogenlike gold following the excitation into the states with $n \leqslant 10$ by collisions with Ar target at 258 MeV/u. The contributions of the different multipoles in the excitation cross sections to the subsequent x-ray emission are shown separately: a monopole (gray-filled area), dipole (dotted-line), quadrupole excitation (yellow-filled area), and sum of all those (solid line).

cross sections are lowered by the magnetic interaction by about 25% for the $ns_{1/2}$ shell, 30% for $np_{1/2}$ and $nd_{3/2}$, and by even 35% for the $np_{3/2}$ and $nd_{5/2}$, rather independent of the principal quantum number n. Small deviations from a *constant* behavior are more likely related to numerical inaccuracies in the four-dimensional integration [cf. expression (3)] rather than due to a true physical dependence of the excitation amplitudes. Note that this reduction appears to be almost identical for the subshells with $j = l - 1/2$ and $j = l + 1/2$ for both the p and d shells and again with only a minor dependence on n.

Further details of the excitation process can be revealed if the cross sections for the Coulomb excitation of hydrogenlike Au^{78+} ions are used to determine the (initial) population of the excited projectile states and an emission spectrum for the corresponding cascade is constructed. Figure 3 displays such a simulated spectrum for the subsequent Lyman series. Apart from the strong Lyman-α_2 and Lyman-α_1 peaks at $\sim$69 and $\sim$71 keV, respectively, the figure shows the higher-energetic Lyman series where states up to $n = 10$ have been considered. The contributions from a monopole (gray-filled area), dipole (dotted line), or quadrupole excitation (yellow-filled area) are shown individually together with their sum (solid line). The monopole excitation is important only for the excitation of the $2s$ (and ns) subshells, while otherwise the dipole excitation dominates as expected. Nevertheless, neither the monopole nor the quadrupole excitations are negligible and are visible in the simulated spectra.

The need of a full inclusion of the Liénard-Wiechert potential can be seen from Fig. 4. Here a comparison between

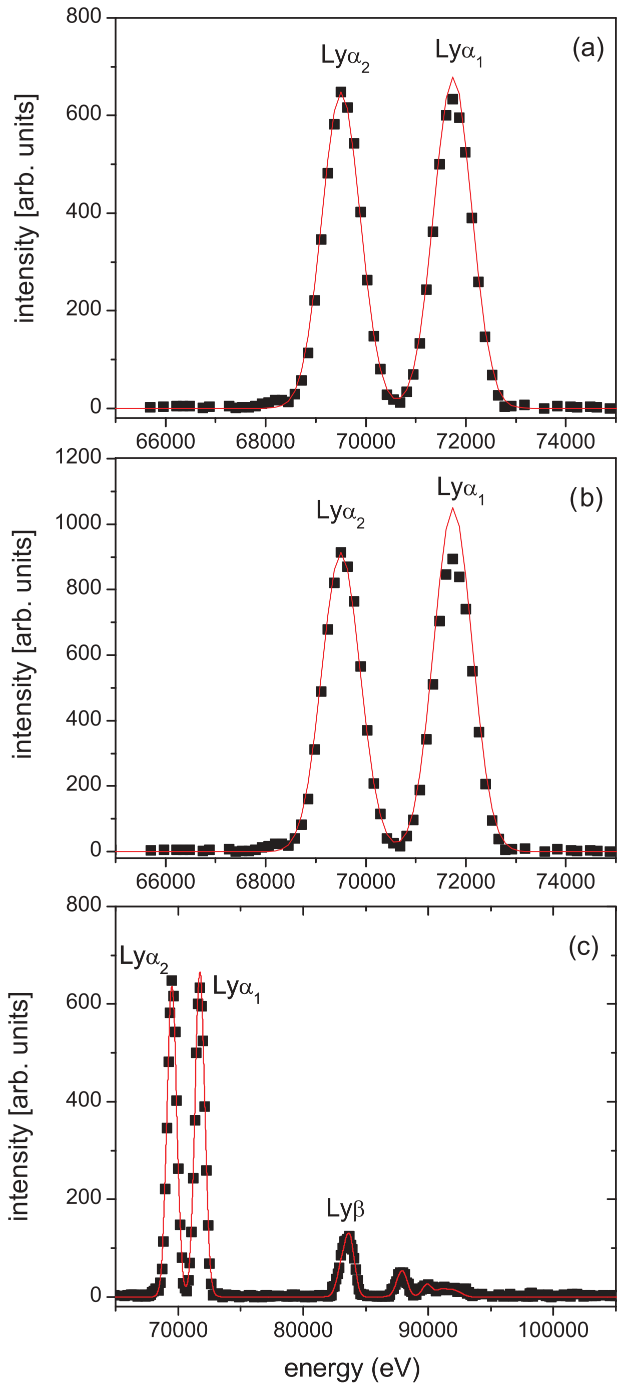

FIG. 4. (Color online) Comparison of the observed and theoretical (simulated) x-ray spectra of hydrogenlike Au^{78+} ions after Coulomb excitation with an Ar jet target. The experimental spectra are normalized to the simulated one by using the Lyman-α_2 line. The simulated spectra include (a) the full relativistic Liénard-Wiechert potential and (b) only the electric part in the computations. In addition, (c) a comparison with the simulated spectra based on the full relativistic Liénard-Wiechert potential is presented for the complete Lyman series.

the experimental and theoretical (simulated) spectra is shown. The energy scale is transformed into the emitter frame. Note that the comparison is not on the absolute scale; for presentation purposes the experimental spectrum is normalized to the theoretical one by adjusting to the simulated Lyman-α_2 line. Good agreement between the simulated and observed spectra are obtained only if, in addition to the electric part in the Liénard-Wiechert potential, we also include the magnetic contributions. We also note that the intensity of the x-ray lines in the simulated spectra varies considerably when comparing Figs. 4(a) and (b).

TABLE I. Comparison of the measured Lyman-α differential cross sections for collisions of H-like Au ions with Ar target at 258 MeV/u with the theoretical predictions, for 35° and 150° angles with respect to the ion beam. All values are in barn/ster.

Angle with respect to ion momentum	35°	150°
Experiment	55.8 ± 2.8	54.9 ± 2.8
Theory (electric part only)	88.3	88.3
Theory (complete calculations)	57.1	57.1

Overall, an excellent agreement is found if the full Liénard-Wiechert potential as well as the cascade contributions from the higher subshells are taken into account. In contrast, the theory overestimates the x-ray emission if only the electric part is considered in calculating the excitation amplitudes. Moreover, we also obtained Lyman-α differential cross sections utilizing a normalization on the K-shell radiative electron capture (K-REC) transition observed in the same experiment and relying on theoretical calculations for this process. This technique has already been successfully used in previous studies [6]. In Table I, a comparison of the obtained values with theoretical predictions is shown. One can clearly see that the use of only the electric part of the interaction potential overestimates the cross section by 50%, whereas the calculations including the full Liénard-Wiechert potential agree well with the experimental results within the error bars.

V. SUMMARY AND OUTLOOK

In conclusion, the projectile excitation of 258 MeV/u hydrogenlike gold ions in collisions with the Ar jet target has been investigated. The x-ray spectra from the projectile excitation have been separated from the x-ray emission due to electron capture into the excited states utilizing an anticoincidence technique. Coulomb excitation from the ground state into the fine-structure-resolved $n = 2$ levels as well as into levels with principal quantum number $n \geqslant 3$ has been measured with excellent statistics. A very good agreement between the observed and simulated spectra is obtained if the calculations are based on Dirac's relativistic equation and a full inclusion of the Liénard-Wiechert potential, whereas the use of only the electric part of the interaction potential overestimates the cross section by 50%. In the upcoming studies, the anticoincidence technique outlined here will be used to explore, in detail, the angular distributions, alignment, and polarization associated with the Coulomb excitation. Furthermore, investigations of Coulomb and electron impact excitation for few-electron systems are planned where the influence of relativity and correlations among the electrons on the projectile excitation can be addressed.

ACKNOWLEDGMENTS

This work was supported by the Alliance Program of the Helmholtz Association (HA216/EMMI). S.F. acknowledges support by the FiDiPro programme of the Finnish Academy and the Deutsche Forschungsgemeinschaft (DFG). A.S. acknowledges support from the Helmholtz Gemeinschaft (Nachwuchsgruppe VH-NG-421).

[1] P. Beiersdorfer, H. Chen, D. B. Thorn, and E. Träbert, Phys. Rev. Lett. **95**, 233003 (2005).
[2] A. Gumberidze *et al.* Phys. Rev. Lett. **94**, 223001 (2005).
[3] Th. Stöhlker, Phys. Scr., T **80A**, 165 (1999).
[4] J. Eichler and Th. Stöhlker, Phys. Rep. **439**, 1 (2007).
[5] S. Fritzsche, P. Indelicato, and Th. Stöhlker, J. Phys. B **38**, S707 (2005).
[6] Th. Stöhlker *et al.* Phys. Rev. A **58**, 2043 (1998).
[7] Th. Stöhlker *et al.* Phys. Scr., T **110**, 384 (2004).
[8] X. Ma, Th. Stöhlker, F. Bosch, O. Brinzanescu, S. Fritzsche, C. Kozhuharov, T. Ludziejewski, P. H. Mokler, Z. Stachura, and A. Warczak, Phys. Rev. A **64**, 012704 (2001).
[9] J. Eichler and W. E. Meyerhof, *Relativistic Atomic Collisions* (Acedemic Press, San Diego, 1995).
[10] C. Brandau *et al.* Phys. Rev. Lett. **89**, 053201 (2002).
[11] Y. Zou, J. R. Crespo López-Urrutia, and J. Ullrich, Phys. Rev. A **67**, 042703 (2003).
[12] P. Beiersdorfer, T. W. Phillips, K. L. Wong, R. E. Marrs, and D. A. Vogel, Phys. Rev. A **46**, 3812 (1992).
[13] Th. Stöhlker *et al.*, Phys. Rev. Lett. **79**, 3270 (1997).
[14] J. H. Scofield, Phys. Rev. A **40**, 3054 (1989).
[15] A. Surzhykov, U. D. Jentschura, Th. Stöhlker, and S. Fritzsche, Phys. Rev. A **73**, 032716 (2006).
[16] A. Surzhykov, U. D. Jentschura, Th. Stöhlker, A. Gumberidze, and S. Fritzsche, Phys. Rev. A **77**, 042722 (2008).
[17] A. Surzhykov, S. Fritzsche, T. Stöhlker, and S. Tachenov, Phys. Rev. A **68**, 022710 (2003).
[18] S. Tashenov *et al.*, Phys. Rev. Lett. **97**, 223202 (2006).
[19] J. Rzadkiewicz *et al.*, Phys. Rev. A **74**, 012511 (2006).
[20] S. Trotsenko *et al.*, Phys. Rev. Lett. **104**, 033001 (2010).
[21] D. Detleffsen, M. Anton, A. Werner, and K. H. Schartner, J. Phys. B **27**, 4195 (1994).
[22] K. Reymann, K. H. Schartner, B. Sommer, and E. Träbert, Phys. Rev. A **38**, 2290 (1988).
[23] M. Anton, D. Detleffsen, K. H. Schartner, and A. Werner, J. Phys. B **26**, 2005 (1993).
[24] N. Stolterfoht, J. Electron Spectrosc. Relat. Phenom. **67**, 309 (1993).
[25] N. Stolterfoht, A. Mattis, D. Schneider, G. Schiwietz, B. Skogvall, B. Sulik, and S. Ricz, Phys. Rev. A **51**, 350 (1995).
[26] K. Wohrer, A. Chetioui, J. P. Rozet, A. Jolly, F. Fernandez, C. Stephan, B. Brendle, and R. Gayet, J. Phys. B **19**, 1997 (1986).
[27] L. Adoui *et al.*, Nucl. Instrum. Methods B **98**, 312 (1995).
[28] D. Vernhet, J. P. Rozet, K. Wohrer, L. Adoui, C. Stephan, A. Cassimi, and J. M. Ramillion, Nucl. Instrum. Methods B **107**, 71 (1996).
[29] B. Brendle, R. Gayet, J. P. Rozet, and K. Wohrer, Phys. Rev. Lett. **54**, 2007 (1985).
[30] H. Chen and P. Beiersdorfer, Can. J. Phys. **86**, 55 (2008).
[31] D. B. Thorn, P. Beiersdorfer, G. V. Brown, R. L. Kelley, C. A. Kilbourne, and F. S. Porter, J. Phys.: Conf. Ser. **163**, 012036 (2009).
[32] Th. Stöhlker *et al.*, Phys. Rev. A **57**, 845 (1998).
[33] Th. Stöhlker, D. C. Ionescu, P. Rymuza, F. Bosch, H. Geissel, C. Kozhuharov, T. Ludziejewski, P. H. Mokler, C. Scheidenberger, and Z. Stachura, Phys. Lett. A **238**, 43 (1998).
[34] D. C. Ionescu and Th. Stöhlker, Phys. Rev. A **67**, 022705 (2003).
[35] S. Fritzsche, J. Electron Spectrosc. Relat. Phenom. **114-116**, 1155 (2001).
[36] A. B. Voitkiv, B. Najjari, and J. Ullrich, Phys. Rev. A **75**, 062716 (2007).
[37] B. Najjari and A. B. Voitkiv, J. Phys. B, At. Mol. Opt. Phys. **41**, 115202 (2008).
[38] A. B. Voitkiv, Phys. Rep. **392**, 191 (2004).
[39] C. Scheidenberger, Th. Stöhlker, W. E. Meyerhof, H. Geissel, P. H. Mokler, and B. Blank, Nucl. Instrum. Methods B **142**, 441 (1998).
[40] Th. Stöhlker *et al.*, Nucl. Instrum. Methods B **61**, 408 (1991).
[41] P. Rymuza *et al.*, J. Phys. B, At. Mol. Opt. Phys. **26**, L169 (1993).
[42] R. Anholt and H. Gould, Adv. At. Mol. Phys. **22**, 315 (1986).
[43] R. Anholt and W. E. Meyerhof, Phys. Rev. A **33**, 1556 (1986).
[44] R. Anholt, W. E. Meyerhof, X. Y. Xu, H. Gould, B. Feinberg, R. J. McDonald, H. E. Wegner, and P. Thieberger, Phys. Rev. A **36**, 1586 (1987).
[45] Th. Stöhlker, D. C. Ionescu, P. Rymuza, T. Ludziejewski, P. H. Mokler, C. Scheidenberger, F. Bosch, B. Franzke, H. Geissel, and O. Klepper, Nucl. Instrum. Methods B **124**, 160 (1997).
[46] A. Krämer, A. Kritzer, H. Reich, and Th. Stöhlker, Nucl. Instrum. Methods B **174**, 205 (2001).
[47] P. A. Amundsen and K. Aashamar, J. Phys. B **14**, 4047 (1981).
[48] A. Messiah, *Quantum Mechanics II* (North-Holland, Amsterdam, 1974).
[49] I. P. Grant, J. Phys. B **19**, 3187 (1986).
[50] S. Fritzsche, A. Surzhykov, and Th. Stöhlker, Nucl. Instrum. Methods B **205**, 469 (2003).
[51] S. Fritzsche, Th. Stöhlker, O. Brinzanescu, and B. Fricke, Hyperfine Interact. **127**, 257 (2000).
[52] Th. Stöhlker, F. Bosch, R. W. Dunford, C. Kozhuharov, T. Ludziejewski, P. H. Mokler, Z. Stachura, P. Swiat, and A. Warczak, Phys. Scr., T **80**, 379 (1999).
[53] S. Fritzsche and Th. Stöhlker, Phys. Scr., T **92**, 311 (2001).